Oxide Solubility Minimum in Liquid Fe-*M*-O Alloy

YOUN-BAE KANG

The origin of the solubility minimum of oxide (M_xO_y) in liquid Fe-*M*-O alloy was investigated, and the minimum was predicted based on thermodynamic calculations. Due to the characteristic property of activities of *M* and O in the liquid, a maximum exists in the product between the two activities if the affinity of *M* to O is significantly high, as most deoxidizing elements are. A *critical activity product* is defined, which is an indicator of the solubility minimum of the M_xO_y in the liquid Fe-*M*-O alloy according to the following relationship: $\max(a_M^x \times a_O^y) = K_{M_xO_y} \times a_{M_xO_y}$, where the $a_{M_xO_y}$ is unity if the alloy is in equilibrium with the pure M_xO_y. The origin of the solubility minimum was explained using the change of the activity product by composition. Available CALPHAD assessments for several binary Fe-*M* liquid alloys and Wagner's solvation shell model were combined to calculate the activity product in the Fe-*M*-O alloy, which can be used to predict the solubility minimum of M_xO_y. A favorable agreement was obtained when *M* = Al, B, Cr, Mn, Nb, Si, Ta, Ti, V, and Zr. The Gibbs energy of dissolution of O in pure liquid *M* ($\Delta g^\circ_{\underline{O}(M)}$) and the Gibbs energy of the formation of M_xO_y per mole of atoms ($\Delta g^\circ_{M_xO_y}/(x+y)$) play important roles in determining the solubility minimum, as long as an interaction between Fe and *M* is less significant than the interaction between metal (Fe and *M*) and O. Predictions of the solubility minima of CaO and MgO were not satisfactory, requiring further improvement of the present analysis.

https://doi.org/10.1007/s11663-019-01663-4

I. INTRODUCTION

PRODUCTION of liquid metal including clean steel requires removal of impurities during the liquid metal processing. In particular, various kinds of gaseous impurities such as O, S, N, and H should be controlled as low as possible before casting of the metal. In a steelmaking process, N and H are removed as gas molecules under low pressure (RH process or vacuum degasser). On the other hand, O and S are removed by chemical reaction using metallic elements that form stable oxide and sulfide. As one of the typical reactions, a deoxidation reaction using Al in liquid Fe is written as:

$$Al_2O_3(s) = 2\underline{Al} + 3\underline{O}; \quad \Delta g_{(1)} = \Delta g^\circ_{(1)} + RT\ln Q_{(1)} \quad [1]$$

where $\underline{Al}$ and $\underline{O}$ are Al and O dissolved in the liquid Fe. $\Delta g_{(1)}$, $\Delta g^\circ_{(1)}$, and $Q_{(1)}$ are the Gibbs energy change, the standard Gibbs energy change, and the equilibrium quotient of Reaction [1], respectively. The Gibbs energy change $\Delta g_{(1)}$ is:

$$\begin{aligned}\Delta g_{(1)} &= 2g_{\underline{Al}} + 3g_{\underline{O}} - g_{Al_2O_3(s)} \\ &= 2(g^\circ_{\underline{Al}} + RT\ln a_{\underline{Al}}) + 3(g^\circ_{\underline{O}} + RT\ln a_{\underline{O}})\end{aligned} \quad [2]$$

$$- (g^\circ_{Al_2O_3(s)} + RT\ln a_{Al_2O_3(s)}) \quad [3]$$

$$= (2g^\circ_{\underline{Al}} + 3g^\circ_{\underline{O}} - g^\circ_{Al_2O_3(s)}) + RT\ln\frac{a^2_{\underline{Al}}a^3_{\underline{O}}}{a_{Al_2O_3(s)}} \quad [4]$$

$$= \Delta g^\circ_{(1)} + RT\ln Q_{(1)} \quad [5]$$

where $g_{\underline{Al}}$, $g_{\underline{O}}$, $a_{\underline{Al}}$, and $a_{\underline{O}}$ are the partial Gibbs energies and the activities of Al and O dissolved in the liquid Fe, $g^\circ_{\underline{Al}}$ and $g^\circ_{\underline{O}}$ are the standard Gibbs energies of the Al and the O, $g_{Al_2O_3(s)}$ and $g^\circ_{Al_2O_3(s)}$ are the partial Gibbs energy of Al_2O_3 in the deoxidation product and the standard Gibbs energy of Al_2O_3, respectively. If the deoxidation product is a pure solid Al_2O_3, $g_{Al_2O_3(s)} = g^\circ_{Al_2O_3(s)}$ and $a_{Al_2O_3(s)} = 1$.

At equilibrium, $\Delta g_{(1)} = 0$, then $Q_{(1)}$ becomes $K_{(1)}$, the equilibrium constant of Reaction [1]:

YOUN-BAE KANG are with the Graduate Institute of Ferrous Technology, Pohang University of Science and Technology, 77 Cheongamro, Namgu, Pohang, Kyungbuk 37673, Republic of Korea and also with the CRCT, Department of Chemical Engineering, École Polytechnique de Montréal, Montreal, QC, H3C 3A7, Canada. Contact e-mail: ybkang@postech.ac.kr

Manuscript submitted February 18, 2019.
Article published online September 4, 2019.

$$K_{(1)} = \frac{a_{\underline{\mathrm{Al}}}^2 a_{\underline{\mathrm{O}}}^3}{a_{\mathrm{Al_2O_3(s)}}} = \exp\left(-\frac{(2g^\circ_{\underline{\mathrm{Al}}} + 3g^\circ_{\underline{\mathrm{O}}} - g^\circ_{\mathrm{Al_2O_3(s)}})}{\mathrm{R}T}\right) \quad [6]$$

The numerical value of each activity depends on the choice of the reference state (the standard Gibbs energy) of each component. Raoultian, Henrian, or 1 wt pct standard state has been widely used.

The activities in Eq. [6] are further expressed:

$$K_{(1)} = \frac{a_{\underline{\mathrm{Al}}}^2 a_{\underline{\mathrm{O}}}^3}{a_{\mathrm{Al_2O_3(s)}}} = \frac{(\gamma_{\underline{\mathrm{Al}}} X_{\mathrm{Al}})^2 (\gamma_{\underline{\mathrm{O}}} X_{\mathrm{O}})^3}{a_{\mathrm{Al_2O_3(s)}}} \quad [7]$$

Activity coefficients of Al ($\gamma_{\underline{\mathrm{Al}}}$) and O ($\gamma_{\underline{\mathrm{O}}}$) are often described by Wagner's interaction parameter formalism[1]:

$$\ln \gamma_{\underline{\mathrm{Al}}} = \epsilon_{\mathrm{Al}}^{\mathrm{Al}} X_{\mathrm{Al}} + \epsilon_{\mathrm{Al}}^{\mathrm{O}} X_{\mathrm{O}} + \rho_{\mathrm{Al}}^{\mathrm{Al}} X_{\mathrm{Al}}^2 + \rho_{\mathrm{Al}}^{\mathrm{O}} X_{\mathrm{O}}^2 + \cdots \quad [8]$$

$$\ln \gamma_{\underline{\mathrm{O}}} = \epsilon_{\mathrm{O}}^{\mathrm{O}} X_{\mathrm{O}} + \epsilon_{\mathrm{O}}^{\mathrm{Al}} X_{\mathrm{Al}} + \rho_{\mathrm{O}}^{\mathrm{O}} X_{\mathrm{O}}^2 + \rho_{\mathrm{O}}^{\mathrm{Al}} X_{\mathrm{Al}}^2 + \cdots \quad [9]$$

where ϵ_i^j and ρ_i^j are the first- and second-order interaction parameters, respectively. Under a condition of Al_2O_3 saturation (equilibrium with the solid Al_2O_3), Al and O contents in the liquid Fe can be obtained by solving a series of equations (Eqs. [6] through [9]) along with the known equilibrium constant and the interaction parameters.

How much those gas impurities can be removed during liquid metal processing is practically important. In particular, for deoxidation, it can be used to approximate the amount of deoxidizer required to achieve the minimum O content. Determination of the deoxidation equilibria in liquid Fe by various deoxidizing elements M(= Al, Cr, Mn, Si, *etc.*) has been a subject of long-time research. The deoxidation equilibria (in other words, the solubility limit of the metal oxide M_xO_y) have been determined through an enormous number of experimental investigations and have been analyzed by theoretical approaches. Well-known compilations of the interaction parameters can be found in the literature.[2–4]

Much experimental evidence has shown that the O content in deoxidation equilibria decreases first, but it increases again while the M content increases. Therefore, a *minimum* exists in the O content, or, in other words, there is a solubility minimum. Some researchers reported that even a maximum may exist in the O content.[5,6] Due to experimental uncertainty (experiments at high temperature dealing with reactive metals, the analytical limit for low O content, overestimation of M and O contents due to entrapment of small oxide particles during sampling for chemical analysis, *etc.*), the location of the minimum and existence of the maximum have been controversial. Nevertheless, improved experimental and analytical techniques allow one to estimate the location of the minimum with a certain uncertainty, although the existence of the maximum is not supported.

There have been theoretical approaches that explain deoxidation equilibria in liquid Fe by various M. The Wagner's interaction parameter formalism has been the most widely used,[1] and the interaction parameters up to second-order terms (ϵ_i^j, ρ_i^j, $\rho_i^{j,k}$ on a mole fraction basis or e_i^j, r_i^j, $r_i^{j,k}$ on a weight percent basis) were determined using measured experimental data for the deoxidation equilibria. With the formalism and the interaction parameters, the minimum of the deoxidation equilibria was predicted.[7–11]

St. Pierre and Blackburn[7] proposed a simple relationship between the first-order interaction parameter and composition of an oxide solubility minimum in the framework of Wagner's interaction parameter formalism.[1] By taking a differential of Eq. [7] with respect to X_{Al}, setting the differential of $K_{(1)}$ and $a_{\mathrm{Al_2O_3(s)}}$ zero, and substituting $\gamma_{\underline{\mathrm{Al}}}$ and $\gamma_{\underline{\mathrm{O}}}$ up to first order, the following relationship was obtained:

$$\left(\frac{\partial X_{\mathrm{O}}}{\partial X_{\mathrm{Al}}}\right)_{T,P} = -\frac{2/X_{\mathrm{Al}} + 2\epsilon_{\mathrm{Al}}^{\mathrm{Al}} + 3\epsilon_{\mathrm{O}}^{\mathrm{Al}}}{3/X_{\mathrm{O}} + 3\epsilon_{\mathrm{O}}^{\mathrm{O}} + 2\epsilon_{\mathrm{Al}}^{\mathrm{O}}} \quad [10]$$

By setting $\frac{\partial X_{\mathrm{O}}}{\partial X_{\mathrm{Al}}} = 0$, the composition of the minimum could be obtained. Including the second-order parameters in Eqs. [8] and [9] would yield not only a minimum but also a maximum in the deoxidation equilibria.[8,12]

The above approach is based on the interaction parameter formalism, which is generally valid in the dilute region of M and O. At high M content, the formalism often fails. Therefore, Eq. [10] would not be valid at high Al content. The approach is also a mathematical treatment to find an extremum point on the calculated deoxidation equilibria. Indeed, with this approach, St. Pierre and Blackburn could not find a minimum in the case of Si deoxidation.[7] They noted that solubility minima of various M_xO_y were predicted if $(\epsilon_M^M + \frac{y}{x}\epsilon_{\mathrm{O}}^M) < 1$, which is not obeyed by interaction parameters concerning Si (M = Si). However, according to the recent experimental study by Shibaev *et al.*,[13] a solubility minimum was found in the non-dilute region of Si. To investigate the solubility minimum at high M content, using the conventional Wagner interaction parameter formalism may not be adequate. As will be shown later, solubility minima of oxides in a number of liquid Fe-M-O exist in relatively high M content (> 1 wt pct, M = Cr, Mn, Nb, Si, Ta, V) where the Wagner interaction parameter formalism may not be valid.

In some alloys with M showing extremely strong affinity to O (such as Al, Ca, Mg, or Zr), the interaction parameter formalism often fails to explain the deoxidation equilibria. Too negative ϵ_i^j (or e_i^j) results in a minimum at lower M content than available experimental data. It was attempted to correct this failure by setting ρ_i^j (or r_i^j) to be positive.[14] This resulted in partial success by shifting the minimum toward higher M content. However, this caused an unexpected maximum on the deoxidation equilibria, which was not supported

by the experiments. This failure is due to assuming an ideal mixing between solutes, although there is a strong attraction between O and M. To account for the strong affinity of M to O, the presence of several associates[15,16] was used in the unified interaction parameter formalism.[17,18] This model could be applicable to less dilute regions, contrary to Wagner's interaction parameter formalism. An explanation of the origin of the solubility minimum was provided using the formation of associate in a context of equilibria among oxide, associate, and solute.[16]

Recently, a quasichemical approach was used to model the Gibbs energy of a liquid Fe-Al-O alloy.[19] It takes into account the strong interaction between O and Al by using the modified quasichemical model (MQM).[20] In this model, the formation of an (Al-O) pair is considered, which is similar to the formation of Al*O associate in the associate model[16,17] at relatively low Al content. However, the MQM is valid over the whole composition range of Al. A successful explanation of Al_2O_3 solubility in liquid Fe-Al-O alloy was realized. A calculated solubility of Al_2O_3 in the alloy at 1873 K (1600 °C) using the MQM is shown in Figure 1. Agreement with the available experimental data can be found in References 19 and 21 In this model, the following three First-Nearest-Neighbor (FNN) pair exchange reactions are considered:

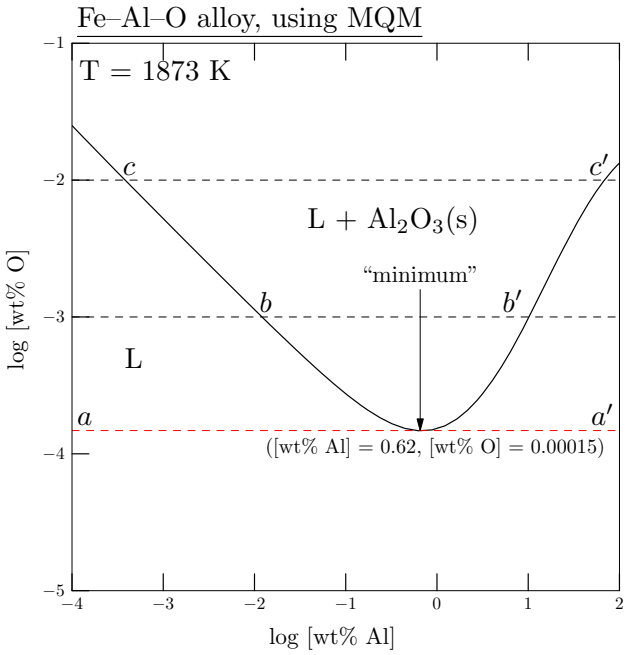

Fig. 1—Solubility of Al_2O_3 in liquid Fe-Al-O alloy at 1873 K (1600 °C) calculated using the modified quasichemical model.[19] Horizontal dashed lines represent 0.00015 ($a-a'$), 0.001 ($b-b'$), and 0.01($c-c'$) wt pct O, respectively.

$$(\text{Fe-Fe}) + (\text{O-O}) = 2(\text{Fe-O}); \quad \Delta g_{\text{FeO}} \qquad [11]$$

$$(\text{Al-Al}) + (\text{O-O}) = 2(\text{Al-O}); \quad \Delta g_{\text{AlO}} \qquad [12]$$

$$(\text{Fe-Fe}) + (\text{Al-Al}) = 2(\text{Fe-Al}); \quad \Delta g_{\text{FeAl}} \qquad [13]$$

where $(i-j)$ and Δg_{ij} are the $(i-j)$ FNN pair and the non-configurational Gibbs energy change for the formation of two moles of $(i-j)$ pairs. The Gibbs energy of mixing of the Fe-Al-O ternary liquid alloy is given by:

$$G = (n_{\text{Fe}} g^{\circ}_{\text{Fe}} + n_{\text{Al}} g^{\circ}_{\text{Al}} + n_{\text{O}} g^{\circ}_{\text{O}}) - T\Delta S^{\text{config}} + \frac{n_{\text{FeAl}}}{2}\Delta g_{\text{FeAl}} + \frac{n_{\text{FeO}}}{2}\Delta g_{\text{FeO}} + \frac{n_{\text{AlO}}}{2}\Delta g_{\text{AlO}} \qquad [14]$$

where g°_i, n_i, n_{ij}, and ΔS^{config} are the molar Gibbs energy of pure liquid i, the number of moles of the i, the number of moles of the $(i-j)$ pair, and an approximate expression for the configurational entropy of mixing given by randomly distributing the six FNN pairs in the one-dimensional Ising approximation.[20] The Δg_{FeO}, Δg_{AlO}, and Δg_{FeAl} may be expanded in terms of pair fractions.[22] Detailed expression of the ΔS^{config}, Δg_{FeO}, Δg_{AlO}, and Δg_{FeAl} can be found elsewhere.[19] Along with the Gibbs energy of a solid Al_2O_3 given by Eriksson and Pelton,[23] a solubility curve of the Al_2O_3 in the liquid Fe-Al-O alloy can be obtained by minimizing the Gibbs energy of the whole system. A solubility minimum was found at $[\text{wt pctAl}] = 0.62, [\text{wt pct O}] = 0.00015$. This falls in the range of a reported minimum of the Al_2O_3 solubility.[21,24] Since this approach is valid at the whole composition range and is well suited to treat the strong affinity of metallic elements to O, finding the solubility minimum of oxide is possible in a reasonable manner. However, this approach has only been applied in limited cases (Fe-M-O system when M = Al[19] and Mn[25]) so far. Therefore, it is not possible to predict the solubility minima of various kinds of M_xO_y until a CALPHAD-type thermodynamic modeling using the quasichemical approach is done. This requires a critical assessment of all available experimental data for all stable phases.

In the present study, a simple approach, but one that is applicable to various systems, is introduced to provide the solubility minima of various oxides in liquid Fe-M-O alloys. First, finding the condition of the solubility minimum from the thermodynamic point of view is attempted. Then, a new method is proposed to predict the solubility minimum using the available CALPHAD modeling for Fe-M binary alloy and Wagner's solvation shell model[26] for an infinite dissolution of O in the Fe-M binary alloy along with a correlation proposed by Chiang and Chang for the exchange energy of solvation shells.[27] By comparing the available experimental data

for the solubility minima, the reliability of the present method is confirmed. Moreover, important properties that determine the solubility minimum are discussed.

II. THERMODYNAMIC CONDITION OF THE SOLUBILITY MINIMUM

By taking pure solid Al_2O_3, pure liquid Al, and pure O_2 gas at 1 bar as reference states of Al_2O_3(s), Al, and O, respectively, the equilibrium constant of Reaction [1] is obtained by the Gibbs energy difference among those pure components ($g^\circ_{Al_2O_3(s)}$, $g^\circ_{Al(l)}$, and $\frac{1}{2}g^\circ_{O_2(g)}$, respectively).

$$K_{(1)} = \frac{a_{Al}^2 a_O^3}{a_{Al_2O_3(s)}} = \exp\left(-\frac{\left(2g^\circ_{Al(l)} + \frac{3}{2}g^\circ_{O_2(g)} - g^\circ_{Al_2O_3(s)}\right)}{RT}\right) \quad [15]$$

The above equilibrium constant is the same as the equilibrium constant of the following reaction involving pure components:

$$Al_2O_3(s) = 2Al(l) + \frac{3}{2}O_2(g); \quad K_{Al_2O_3} \quad [16]$$

$$K_{Al_2O_3} = \frac{a_{Al}^2\left(\frac{P_{O_2}}{P^\circ_{O_2}}\right)^{\frac{3}{2}}}{a_{Al_2O_3(s)}} = \exp\left(-\frac{\left(2g^\circ_{Al(l)} + \frac{3}{2}g^\circ_{O_2(g)} - g^\circ_{Al_2O_3(s)}\right)}{RT}\right) \quad [17]$$

where P_{O_2} and $P^\circ_{O_2}$ are the partial pressure of O_2 over the liquid Fe(-Al-O alloy) and the pressure of O_2 at its reference state, respectively. Therefore, the deoxidation equilibrium of Reaction [1] can be represented by $K_{Al_2O_3}$ (the equilibrium constant of Reaction [16] involving the pure components) by taking pure solid Al_2O_3, pure liquid Al, and pure O_2 gas at 1 bar as the reference states of Al_2O_3, Al, and O, respectively. The activity of O in the liquid Fe alloy is defined as:

$$a_O = \sqrt{\frac{P_{O_2}}{P^\circ_{O_2}}} \quad [18]$$

From Eq. [15], an activity product between a_{Al} and a_O is written as:

$$a_{Al}^2 a_O^3 = K_{(1)} \times a_{Al_2O_3(s)} = K_{Al_2O_3} \times a_{Al_2O_3(s)} \quad [19]$$

where a_{Al} is written as a_{Al}, as the Al content (X_{Al}) varies from 0 to 1. For the activity product, the following can be considered:

- When the liquid Fe-Al-O alloy is in equilibrium with the solid Al_2O_3, $a_{Al_2O_3(s)} = 1$ and $a_{Al}^2 a_O^3$ become $K_{Al_2O_3}$. Otherwise, the activity product $a_{Al}^2 a_O^3$ varies with $a_{Al_2O_3(s)}$ depending on the Al and O contents in the alloy. The solubility curve shown in Figure 1 was calculated at the condition of $a_{Al_2O_3(s)} = 1$. The minimum point also satisfies $a_{Al_2O_3(s)} = 1$.
- The activity product is less than $K_{Al_2O_3}$ when [wt pct O] < 0.00015 at 1873 K (1600 °C) at all Al contents.
- In an infinite dilute region of O, a_{Al} is almost independent of the O content because there is virtually no O to interact with the Al. Or mathematically, using Eq. [8], $X_O \to 0$ results in γ_{Al} (and a_{Al}) to be independent of X_O. Increasing the O content would influence the a_{Al}. However, the low O content at the solubility minimum would not change a_{Al} significantly from the a_{Al} at $X_O \to 0$. Therefore, this condition may be extended to the O content of the solubility minimum.
- At a given O content, a_{Al} must increase as [wt pct Al] increases. On the other hand, a_O would decrease as [wt pct Al] increases because of the higher affinity of Al to O than that of Fe. Therefore, the activity product ($a_{Al}^2 a_O^3$) may exhibit a maximum depending on the composition dependence of both a_{Al} and a_O.

Figure 2 shows the activities of O and Al and their activity product ($a_{Al}^2 a_O^3$) as functions of [wt pct Al] at 1873 K (1600 °C) at three different O contents. These were calculated from the same Gibbs energy equation

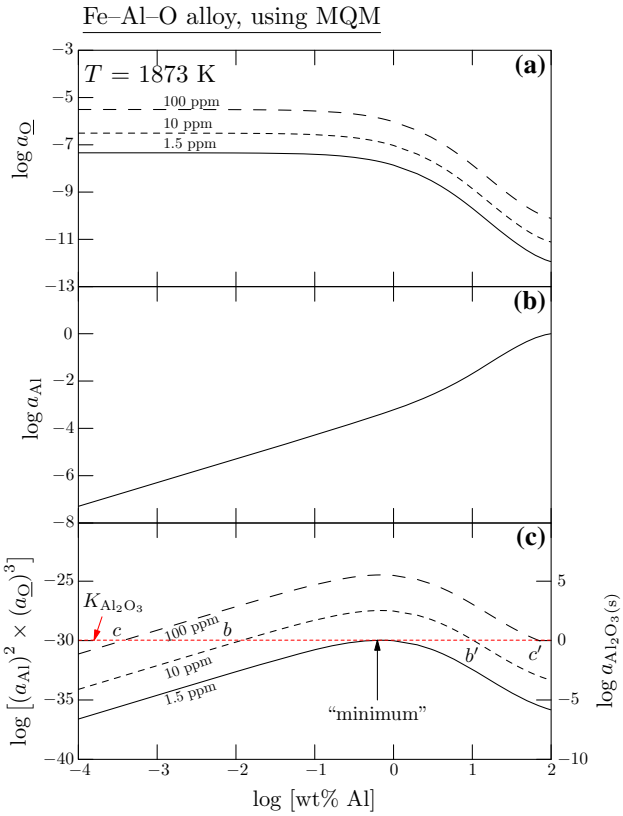

Fig. 2—(*a*) Activity of O (with respect to pure O_2(g) at 1 bar), (*b*) activity of Al (with respect to pure liquid Al), and (*c*) activity product of Fe-Al-O alloy at various oxygen contents ([wt pct O] = 0.00015, 0.001, and 0.01) at 1873 K (1600 °C), calculated using the modified quasichemical model.[19] [wt pct Al] at the points *b*, *b*′, *c*, *c*′, and "minimum" are the same as those in Fig. 1. $K_{Al_2O_3}$ is the equilibrium constant of Reaction [16].

used in Figure 1. Changes of the $a_{\underline{O}}$ and the a_{Al} with respect to the Al content are obvious, and the activity product shows a maximum at each oxygen content. Figure 2(c) shows that the higher O content results in a higher activity product over the entire Al content. Therefore, the maximum of the activity product of a higher O content is higher than that of a lower O content. A horizontal dotted line in Figure 2(c) represents $K_{Al_2O_3}$, which intersects with the activity product curve at a point ([wt pct O] = 0.00015) or two points ([wt pct O] = 0.001, 0.01), respectively. Al contents at the "minimum," b, b', c, and c' are identical to those in Figure 1. The solid curve in Figure 2(c) is the activity product $a_{Al}^2 a_{\underline{O}}^3$ along the $a - a'$ in Figure 1 ([wt pct O] = 0.00015). Since the maximum value of the activity product at [wt pct O] = 0.00015 is exactly the same as $K_{Al_2O_3}$ (marked by an upward arrow "minimum"), according to Eq. [19], $a_{Al_2O_3(s)} = 1$ only at the specific Al content ([wt pctAl] = 0.62). The $a_{Al}^2 \times a_{\underline{O}}^3$ at this specific composition may be called a *critical* activity product. Except for this point, $a_{Al_2O_3(s)} < 1$ at this O content ([wt pct O] = 0.00015): the liquid alloy is not in equilibrium with the Al_2O_3(s).

At higher O content, the activity product is higher than $K_{Al_2O_3}$ in a range (within $b - b'$ ([wt pct O] = 0.001) or $c - c'$ ([wt pctO] = 0.01)): Al_2O_3(s) is stable within the range. It is clear that the maximum of the activity product at [wt pct O] = 0.00015 (the critical activity product) corresponds to the condition of the minimum of the solubility of Al_2O_3 in Figure 1.

Consequently, it may be understood that the solubility minimum occurs because of the higher O affinity of Al that lowers the stability of Al_2O_3, which is proportional to $a_{Al}^2 \times a_{\underline{O}}^3$, at high Al content. Such high affinity to O by Al forces keeping O in the liquid alloy by dissociating the solid Al_2O_3. It should be noted that the strong affinity of Al to O occurs in the liquid. When Al is added to a liquid Fe containing O (*e.g.*, 10 ppm in Figure 1), the first choice of the system is to keep O in the liquid to allow strongly short-range ordered O with Al in the liquid. Therefore, the O content in the liquid does not decrease by increasing Al content up to a certain level (at b in Figure 1). Further increasing the Al content makes the short-range ordered liquid structure form a long-range ordered alumina (from a cluster to a crystal). In this case, as O leaves the liquid, the O content in the liquid decreases (following the solid curve from point b in Figure 1). This is what the deoxidation reaction does. However, additionally increasing the Al content to a higher level (passing the solubility minimum) requires forming the short-range ordered liquid structure again because of abundant Al to interact with O. This results in stabilizing O dissolved in the liquid, thereby increasing the O content again.

As long as the O content is low enough not to influence a_{Al} and $\gamma_{\underline{O}} (= a_{\underline{O}}/X_O)$, the shape of the activity product is almost irrespective of the O content. Therefore, the Al content at the maximum of the activity product is not sensitive to the O content, as can be seen in Figure 2.

For a general case in a Fe-M-O alloy,

$$M_xO_y = xM(l) + \frac{y}{2}O_2(g); \quad K_{M_xO_y} \qquad [20]$$

the thermodynamic condition of a solubility minimum is

$$\max(a_M^x a_{\underline{O}}^y) = K_{M_xO_y} \times a_{M_xO_y} \qquad [21]$$

where $a_{M_xO_y} = 1$ for pure M_xO_y. If formulae for the activities of M and O are available as functions of composition, then the solubility minimum can be obtained by the above condition (Eq. [21]) along with the $K_{M_xO_y}$.

A. *Maximum of the Activity Product*

The critical activity product depends on the composition dependence of a_M and $a_{\underline{O}}$ in liquid Fe-M-O alloy. Since a_M and $a_{\underline{O}}$ are determined by the Gibbs energy of mixing of the alloy, occurrence of the solubility minimum (by maximizing the activity product) should be dependent on the interaction energies among the components.

For example, in an $A - B - O$ alloy where B has strong affinity to O, thereby forming "BO(s)":

$$BO(s) = B + O; \quad K_{BO} \qquad [22]$$

an activity product is written as:

$$a_B a_{\underline{O}} = (\gamma_B X_B)(\gamma_{\underline{O}} X_O) \qquad [23]$$

For the sake of simplicity, if the liquid alloy behaves as a regular solution characterized by three interaction energies in each sub-binary system (ω_{AB} for $A - B$, ω_{AO} for $A - O$, and ω_{BO} for $B - O$, respectively), the activity coefficients of B and O can be formulated as follows:

$$RT \ln \gamma_B = \omega_{AB}(1 - X_B)^2 \qquad [24]$$

$$RT \ln \gamma_{\underline{O}} = (1 - X_B)\omega_{AO} + X_B\omega_{BO} - \omega_{AB}(1 - X_B)X_B \qquad [25]$$

in the limit of infinite dilution of O ($X_O \to 0$). By substituting Eqs. [24] and [25] into Eq. [23], the activity product is calculated. Figure 3 shows the activity product (calculated at $X_O = 10^{-4}$ as an example) normalized to its maximum values in each case. ω_{AO} was set to a constant ($-10RT$), while ω_{BO} was varied to determine its impact on the maximum of the activity product. Besides, the interaction in the metal phase (ω_{AB}) was set as either negative (Figure 3(a)) or positive (Figure 3(b)).

In Figure 3(a), ω_{BO} was set to $-5RT$, $-10RT$, $-12RT$, and $-15RT$. When $\omega_{BO} = -12RT$ or $-15RT$, there is a maximum in each case. More negative ω_{BO} puts the maximum at lower X_B. Similar results are seen in Figure 3(b) where ω_{AB} is positive.

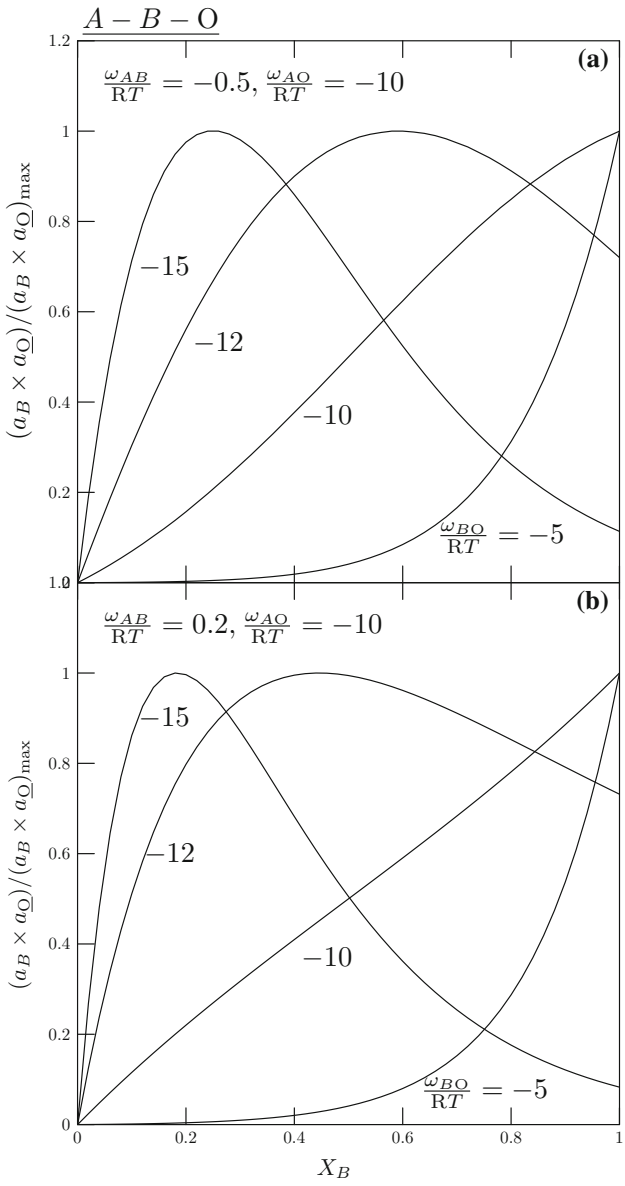

Fig. 3—Activity product normalized by its maximum value in $A-B-O$ ($X_O = 10^{-4}$): (*a*) $\omega_{AB}/RT = -0.5$, $\omega_{AO}/RT = -10$, (*b*) $\omega_{AB}/RT = 0.2$, $\omega_{AO}/RT = -10$. Varying ω_{BO}/RT from −5 to −15 influences the occurrence of the maximum of the activity product.

B. *A Case Where the Solubility Minimum is Not Found*

Figure 3 shows that the maximum of the activity product is not always obtained. When ω_{BO} is less negative ($\omega_{BO} = -5RT$ and $-10RT$), there is no maximum on the activity product. This results in no solubility minimum. When ω_{BO} is negative enough ($\omega_{BO} = -12RT$ and $-15RT$), the maximum on the activity product is found, and this will result in the solubility minimum if the condition is satisfied (Eq. [21]). This is schematically shown in Figure 4. A solid line and a dotted line represent probable cases of the solubility limit of the oxide *B*O (or liquidi of the *B*O on the isothermal section). The solid line shows a minimum of the solubility of *B*O, while the dotted line

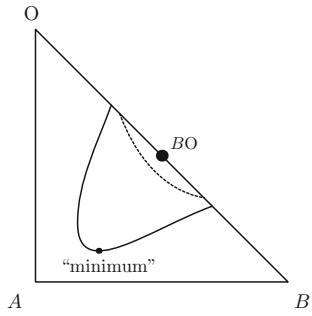

Fig. 4—Schematic figure of an isothermal section of the *A*-*B*-O system, showing saturation of a liquid solution by *B*O. A solid curve shows a "minimum," while a dotted curve does not show a "minimum".

does not show a minimum. It is seen that the solubility minimum does not always occur although the oxide *B*O forms in the liquid. In many cases, a solubility minimum was reported in Fe-*M*-O alloy, because the interaction between *M* and O is strong. However, depending on the interaction, such a solubility minimum may not exist or is shifted toward higher *B* content. Further discussion will be given in Section V–A.

III. CALCULATION OF THE ACTIVITY PRODUCT IN FE-*M*-O ALLOYS

To estimate the solubility minimum of oxide M_xO_y in liquid Fe-*M*-O alloys, the condition in Eq. [21] can be used. If the Gibbs energy model of the liquid Fe-*M*-O alloy is available in a wider composition range (from pure Fe to pure *M* and zero O content up to the oxide saturation limit) to acceptable accuracy, a_M and $a_{\underline{O}}$ can be calculated with high accuracy. Using Eq. [21] along with the $K_{M_xO_y}$, the solubility minimum can be calculated. Application of the CALPHAD calculation is also a way to obtain not only the solubility minimum but also the whole solubility limit of the M_xO_y in the liquid Fe-*M*-O alloy (deoxidation curve). However, the deoxidation equilibria are not easy to model thermodynamically because of the strong interaction between metal and oxygen. Although there are some Gibbs energy models available, thermodynamic optimization using the models to describe the deoxidation equilibria over a wide composition range is still scarce. Even for the Fe-Al-O system, which is one of the most representative liquid steel systems, only one study is available to the best knowledge of the present author,[19] which describes the deoxidation equilibria of Al_2O_3 in the whole composition range (Figure 1). While research on thermodynamic modeling for deoxidation is being carried out, it is worthwhile to find a simple way to estimate the solubility minimum in various steel systems (Fe-*M*-O).

In the present study, to determine the solubility minima of various Fe-*M*-O alloys, Eq. [21] was used. a_M and $a_{\underline{O}}$ were calculated using reasonable thermodynamic models, respectively. a_M in the Fe-*M*-O alloy was approximated to the a_M in the binary Fe-*M* alloy.

Although this is strictly valid at the infinite dilution of O, the present calculation may be a reasonable approximation, since the O content in the Fe-*M*-O alloy at the solubility minimum is low (maximum a few hundred ppm levels) as will be shown later.

A. *Activity of M in Fe-M: CALPHAD*

a_M in the Fe-*M*-O system was approximated to that in the Fe-*M* binary system. The a_M can be obtained by using the thermodynamically assessed Gibbs energy function for the liquid phase. When the Gibbs energy function of the binary Fe-*M* alloy is modeled using a random mixing model, the excess Gibbs energy is described as:

$$g^{\text{ex}} = X_{\text{Fe}} X_M \sum_{i=0} {}^{i}L_{\text{Fe}M}(X_{\text{Fe}} - X_M)^i \qquad [26]$$

where ${}^{i}L_{\text{Fe}M}$ is the model parameter. This is usually obtained by critical evaluation and thermodynamic optimization for available thermodynamic/phase diagram data. From the following relationship:

$$\text{R}T\ln\gamma_M = g^{\text{ex}} + (1 - X_M)\frac{\partial g^{\text{ex}}}{\partial X_M} \qquad [27]$$

$a_M (= \gamma_M X_M)$ can be calculated as a function of X_M.

B. *Activity of O in Fe-M: Solvation Shell Model*

The Henrian activity coefficient of O ($\gamma_{\text{O}}^{\circ}$) was calculated using Wagner's solvation shell model.[26] O is assumed to dissolve in various vacant shells composed of Fe and *M*, as schematically shown in Figure 5. A vacant shell formation is described as:

$$(Z - i)\text{Fe} + iM = V(\text{Fe}_{Z-i}M_i); \Delta g_{iv} \qquad [28]$$

where Z, i, and $V(\text{Fe}_{Z-i}M_i)$ stand for the coordination number of O, the number of *M* atoms in the vacant shell, and the vacant shell composed of $(Z - i)$ Fe and i *M*. Δg_{iv} is the Gibbs energy change of Reaction [28] and is formulated according to Schmid *et al.*[28]:

$$\Delta g_{iv} = \frac{1}{2}(Z - i)ih_{\text{Fe}M} \qquad [29]$$

O dissolves into the vacant shell by the following reaction:

$$\frac{1}{2}\text{O}_2(g) + V(\text{Fe}_{Z-i}M_i) = \text{O}(\text{Fe}_{Z-i}M_i); \Delta g_{i\text{O}} - \Delta g_{iv} \qquad [30]$$

where the $\text{O}(\text{Fe}_{Z-i}M_i)$ stands for the solvation shell of O (an O atom surrounded by $(Z - i)$ Fe atoms and i *M* atoms). $(\Delta g_{i\text{O}} - \Delta g_{iv})$ is the Gibbs energy change of Reaction [30] and is formulated according to Wagner[26] and modified by Schmid *et al.*[28]:

$$\Delta g_{i\text{O}} - \Delta g_{iv} = \frac{Z - i}{Z}\Delta g_{\underline{\text{O}}(\text{Fe})} + \frac{i}{Z}\Delta g_{\underline{\text{O}}(M)} - \frac{1}{2}(Z - i)ih \qquad [31]$$

where $\Delta g_{\underline{\text{O}}(\text{Fe})}$ are $\Delta g_{\underline{\text{O}}(M)}$ are the limiting values of the $\Delta g_{i\text{O}}$ at $i = 0$ and $i = Z$, respectively. These are functions of $\gamma_{\underline{\text{O}}(Fe)}^{\circ}$ and $\gamma_{\underline{\text{O}}(M)}^{\circ}$, respectively. h is the energy difference between the following two vacancy–O exchange reactions ($h = \Delta h_{(i+1)} - \Delta h_{(i)}$):

$$\begin{aligned}&\text{O}(\text{Fe}_{Z-i}M_i) + V(\text{Fe}_{Z-(i+1)}M_{(i+1)})\\ &\quad = V(\text{Fe}_{Z-i}M_i) + \text{O}(\text{Fe}_{Z-(i+1)}M_{(i+1)}); \quad \Delta h_{(i)}\end{aligned} \qquad [32]$$

$$\begin{aligned}&\text{O}(\text{Fe}_{Z-(i+1)}M_{(i+1)}) + V(\text{Fe}_{Z-(i+2)}M_{(i+2)})\\ &\quad = V(\text{Fe}_{Z-(i+1)}M_{(i+1)}) + \text{O}(\text{Fe}_{Z-(i+2)}M_{(i+2)}); \quad \Delta h_{(i+1)}\end{aligned} \qquad [33]$$

Wagner assumed the h to be a constant, as a limiting case of linear dependence of $\Delta h_{(i)}$ on increasing i in the solvation shell.[26] The physical meaning of this

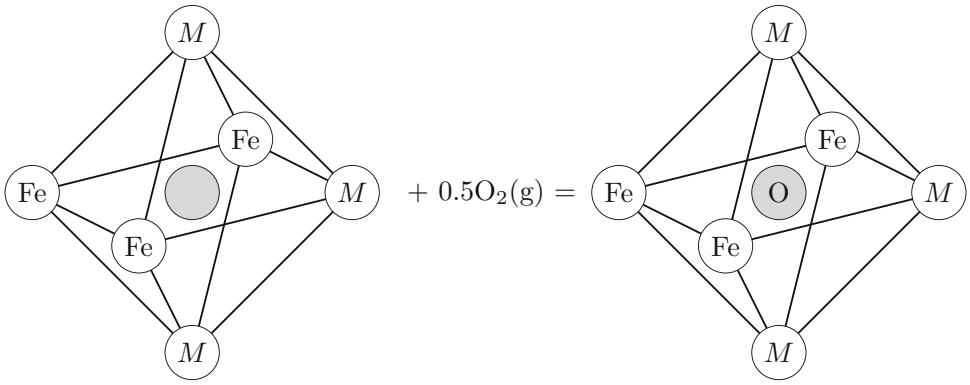

Fig. 5—A schematic representation of the solvation shell model for dissolving O in a liquid Fe-*M* alloy. A gray circle before the reaction represents a vacant shell of $i = 3$ out of $Z = 6$, which is then occupied by O. The Gibbs energy change for this reaction is $\Delta g_{i\text{O}} - \Delta g_{iv}$, for which $\Delta g_{iv} = 0$ was assumed in the present study.

term is that the extent of electron transfer per M atom keeps decreasing gradually and constantly when the number of M atoms in the solvation shell increases. By a mass action law for Reaction [30], Sievert's law, and binomial distribution formula, the Henrian activity coefficient of O ($\gamma_{\underline{O}}^{\circ}$) is obtained as[28]:

$$\gamma_{\underline{O}}^{\circ} = \left(\sum_{i=0}^{Z} \frac{Z!}{(Z-i)!i!} \left[\frac{Y_{Fe}\gamma_{Fe}}{[\gamma_{\underline{O}(Fe)}^{\circ}]^{1/Z}} \right]^{Z-i} \left[\frac{Y_M \gamma_M}{[\gamma_{\underline{O}(M)}^{\circ}]^{1/Z}} \right]^{i} \exp\left[\frac{(Z-i)i}{2RT}(h - h_{FeM}) \right] \right)^{-1} \quad [34]$$

where Y_{Fe} and Y_M are the atomic ratio of metallic components $X_{Fe}/(X_{Fe}+X_M)$ and $X_M/(X_{Fe}+X_M)$, respectively. By setting $h_{FeM}=0$ according to Wagner as a first approximation,[26] Eq. [34] reduces to:

$$\gamma_{\underline{O}}^{\circ} = \left(\sum_{i=0}^{Z} \frac{Z!}{(Z-i)!i!} \left[\frac{Y_{Fe}}{[\gamma_{\underline{O}(Fe)}^{\circ}]^{1/Z}} \right]^{Z-i} \left[\frac{Y_M}{[\gamma_{\underline{O}(M)}^{\circ}]^{1/Z}} \right]^{i} \exp\left[\frac{(Z-i)i}{2RT} h \right] \right)^{-1} \quad [35]$$

The parameter h was empirically formulated by Chiang and Chang[27]:

$$h = \left(\frac{2}{Z^2}\right)\left(\frac{g^{ex}}{Y_{Fe}Y_M}\right) + 0.09\left(\frac{g^{ex}}{Y_{Fe}Y_M}\right)\left(\frac{V_M}{V_{Fe}}\right)^2 + 0.04 \times (\Delta g_{\underline{O}(Fe)}^{\circ} - \Delta g_{\underline{O}(M)}^{\circ}) \quad [36]$$

where V_M and V_{Fe} are the metallic valences for M and Fe, respectively, as given by Pauling.[29] $\Delta g_{\underline{O}(Fe)}^{\circ}(= RT\ln\gamma_{\underline{O}(Fe)}^{\circ})$ and $\Delta g_{\underline{O}(M)}^{\circ}(= RT\ln\gamma_{\underline{O}(M)}^{\circ})$ are the Gibbs energies of dissolution of O in liquid Fe and liquid M at 1 at. pct, respectively:

$$\frac{1}{2}O_2(g) = \underline{O}\ (1\ \text{at. pct in liquid Fe (or } M)) \quad [37]$$

The order of Fe and M in Eq. [36] was set in such a way that $V_{Fe}/V_M > 1$ and $(\ln\gamma_{\underline{O}(Fe)}^{\circ} - \ln\gamma_{\underline{O}(M)}^{\circ}) > 0$.[30,31] In the work of Chiang and Chang,[27] the h was formulated as a function of enthalpy of mixing in the Fe-M alloy. Since the correlation obtained by Chiang and Chang[27] was based on the regular solution assumption for which relevant data were obtained from the compilations of Hultgren *et al.*,[32] it is thought that the excess Gibbs energy may be suitable to replace the enthalpy of mixing. The excess Gibbs energy formulations are available after a series of CALPHAD assessments.[33–44] Chiang and Chang proposed to use a composition dependence of $h(= h_1 + h_2 \times i)$,[27] but such extension was not used in the present study because of a limit of availability of the parameters (h_1, h_2). However, due to the composition dependence of g_{FeM}^{ex} in Eq. [36], h is dependent on the composition in the present study.

Assuming the $\gamma_{\underline{O}}^{\circ} \approx \gamma_{\underline{O}}$ in the region of dilute O, $a_O(= \gamma_{\underline{O}} X_O)$ can be calculated as a function of X_M.

IV. APPLICATION OF THE ACTIVITY PRODUCT CALCULATION IN THE FE-*M*-O SYSTEM (*M* = Al, B, CA, CR, MG, MN, NB, SI, TA, TI, V, ZR)

Solubility minima of M_xO_y in liquid Fe-M-O alloys were predicted as described in Section III (Eqs. [21], [27], and [35]) and compared with available experimental data.

A. *Parameters Used in the Calculation*

The γ_M in Fe-M alloy was calculated using Eq. [27] to obtain a_M. Required ${}^{i}L_{FeM}$ parameters for each Fe-M system were taken from CALPHAD assessments as shown in Table I.[33–44]*.

*γ_M also may be directly obtained by using commercial CALPHAD software and databases in which more sophisticated thermodynamic models may be employed to obtain a better description of g^{ex}.

The $\gamma_{\underline{O}}$ was calculated using Eq. [35] along with the empirical correlation (Eq. [36]). The coordination number Z, metallic valences V_M and V_{Fe} of Pauling[29] were obtained from Chang *et al.*[31] and are listed in Table II. $\Delta g_{\underline{O}(Fe)}^{\circ}(= RT(\ln\gamma_{\underline{O}(Fe)}^{\circ})$ and $\Delta g_{\underline{O}(M)}^{\circ}(= RT\ln\gamma_{\underline{O}(M)}^{\circ})$ were obtained from various sources as listed in Table III. As will be shown in Section V–A, a maximum of the activity product depends more on composition dependence of $\gamma_{\underline{O}}$ ($a_{\underline{O}}$ at a given O content) than a_M. The composition dependence of $\gamma_{\underline{O}}$ depends significantly on $\Delta g_{\underline{O}(M)}^{\circ}$. Therefore, in the present study, all available $\Delta g_{\underline{O}(M)}^{\circ}$ values in the literature were taken into account in the calculation of the solubility minimum.

The equilibrium constant ($K_{M_xO_y}$) for Reaction [20] was obtained from the FactSage FactPS (pure substance) database[45], which is primarily based on the JANAF thermochemical table.[46] $K_{M_xO_y}$ values for various M at 1873 K (1600 °C) are listed in Table IV. It should be noted that the equilibrium oxide phase (M_xO_y) was determined from experimental reports.[13,21,24,47–55] However, the same procedure can be used for other oxide phases such as $Fe_wM_xO_y$ by taking $a_{M_xO_y} \neq 1$ in Eq. [21].

B. *Character of the Solubility Minimum*

In the present study, the solubility minima in various Fe-M-O alloys were thermodynamically predicted and compared with available experimental data, as will be shown in the following sections. Numerous experimental results are available on the solubility of oxides in the liquid Fe alloys. By inspecting the solubility data, the minimum for the solubility was estimated. However, due to the inherent difficulty of the high temperature experiment and uncertainty of the analytical method, experimental uncertainty is inevitable. Also, due to the shape of the solubility limit (concave down around the

Table I. Excess Gibbs Energy Parameters in Fe-*M* Binary Liquid Alloys

M in Fe-*M*	Excess Gibbs Energy Parameter (J mol^{-1})				Reference
	${}^0L_{FeM}$	${}^1L_{FeM}$	${}^2L_{FeM}$	${}^3L_{FeM}$	
Al	$-88090 + 19.8T$	$3800 - 3T$	-2000	0	33
B	$-133438 + 33.95T$	-7771	29739	0	34
Ca	120705	0	0	0	35
Cr	$-14550 + 6.65T$	0	0	0	36
Mg	$61343 + 1.5T$	0	0	0	37
Mn	$-3950 + 0.489T$	1145	0	0	38
Nb	$-73554.99 + 104.28T - 9.984T\ln T$	$20336 - 13.525T$	0	0	39
Si	$-164434.6 + 41.9773T$	$-21.523T$	$-18821.542 + 22.07T$	9695.8	40
Ta	$-54797.3 - 0.9862T$	$1118.4 - 12.3462T$	0	0	41
Ti	$-76247 + 17.845T$	$7990 - 6.059T$	$4345 - 2.844T$	0	42
V	$-35963 + 10.489T$	$-4935 + 6.290T$	0	0	43
Zr	$-87715.09 + 18.69T$	$-20078.73 + 16.27T$	-13743.14	0	44

Table II. Pauling's Metallic Valency and Coordination Number[29,31]

M	Al	B*	Ca	Cr	Fe	Mg	Mn	Nb	Si	Ta	Ti	V	Zr
V_M	3	3	2	6	6	2	6	5	2.56	5	4	5	4
Z	6	6	6	6	6	6	6	6	6	6	6	6	6

*Assumed to be the same as Al.

minimum as seen in Figure 4), the minimum of the solubility limit determined in the experiment has uncertainty in its composition.[56] Wider change in the *M* content is reflected by relatively little variation in the O content around the solubility minimum. Therefore, the estimated experimental uncertainty in the *M* content is included in the present analysis.

C. *Fe-Al-O*

Shown in Figure 6 is the calculated fraction of various solvation shells in the Fe-Al-O alloy at 1873 K (1600 °C)**. Different types of shells are schematically shown above the graph. Note that there are also seven other solvation shells that do not contain O inside (vacant shells). Those vacant shells were not considered in the calculation of the fraction in Figure 6. Increasing Al content rapidly increases the fraction of Al-containing shells because of the higher O affinity of Al.

Figure 7 shows the calculated activity product of the Fe-Al-O alloy at 1873 K (1600 °C) in the present study. Among the various $\Delta g^\circ_{\underline{O}(Al)}$, that of Liang[57] was used, which is the recommended value for the present calculation as will be shown later. Three different X_O were used. It can be seen that the activity product at each X_O shows the maximum, and the Al content of each maximum looks virtually irrespective of the X_O. This supports the assumption used in the present study (a_M in Fe-*M* $\approx$ a_M in Fe-*M*-O, $\gamma_{\underline{O}} \approx \gamma^\circ_O$, both in dilute O content). A horizontal dotted line represents $K_{Al_2O_3}$, and $X_O = 10^{-5.35}$ satisfied Eq. [21] with $a_{Al_2O_3} = 1$. Therefore, the maximum on the activity product at this condition corresponds to the minimum of the Al_2O_3 solubility in the liquid Fe-Al-O alloy at 1873 K (1600 °C) (*critical* activity product). If $X_O > 10^{-5.35}$, the $a_{Al_2O_3}$ (the activity product divided by $K_{Al_2O_3}$) is higher than unity in some Al content range. This is a condition where the liquid alloy is saturated by Al_2O_3. Therefore, in actual thermodynamic equilibrium, the activity product does not increase over the horizontal dotted line.

The calculated solubility minimum of Al_2O_3 at 1873 K (1600 °C) is shown in Figure 8(a) along with the reported solubility minimum (closed circle with an error bar).[21,24] The closed square is a calculated solubility minimum with an estimated $\Delta g^\circ_{\underline{O}(Al)}$, as will be shown later in Section IV–N (Figure 9). Other symbols are the calculated solubility minima with the reported $\Delta g^\circ_{\underline{O}(Al)}$ values in the literature.[30,31,57,58] Among the calculated minima, that with $\Delta g^\circ_{\underline{O}(Al)}$ of Liang[57] is the closest to the experimental data.[21,24] The calculation with the estimated $\Delta g^\circ_{\underline{O}(Al)}$ in the present study also predicted a close O content, but slightly lower Al content compared with the experimental data.[21,24]

**By applying Eq. [35] in the Fe-Al-O system, γ°_O can be calculated as a function of Al content. Since $a_{\underline{O}} = \gamma^\circ_O X_O$, $X_O = \frac{a_O}{\gamma^\circ_O} = a_{\underline{O}}(\sum_{i=0}^{Z}(\cdots))$ where $\cdots$ is the term inside the summation in Eq. [35]. This term is contributed from each solvation shell of i (i = 0 to 6 in the present study). Therefore, X_O has seven contributions from the seven different solvation shells, respectively. X_O from each contribution is normalized to the overall X_O ($= a_{\underline{O}}(\sum_{i=0}^{Z}(\cdots))$, and it represents the fraction of each solvation shell.

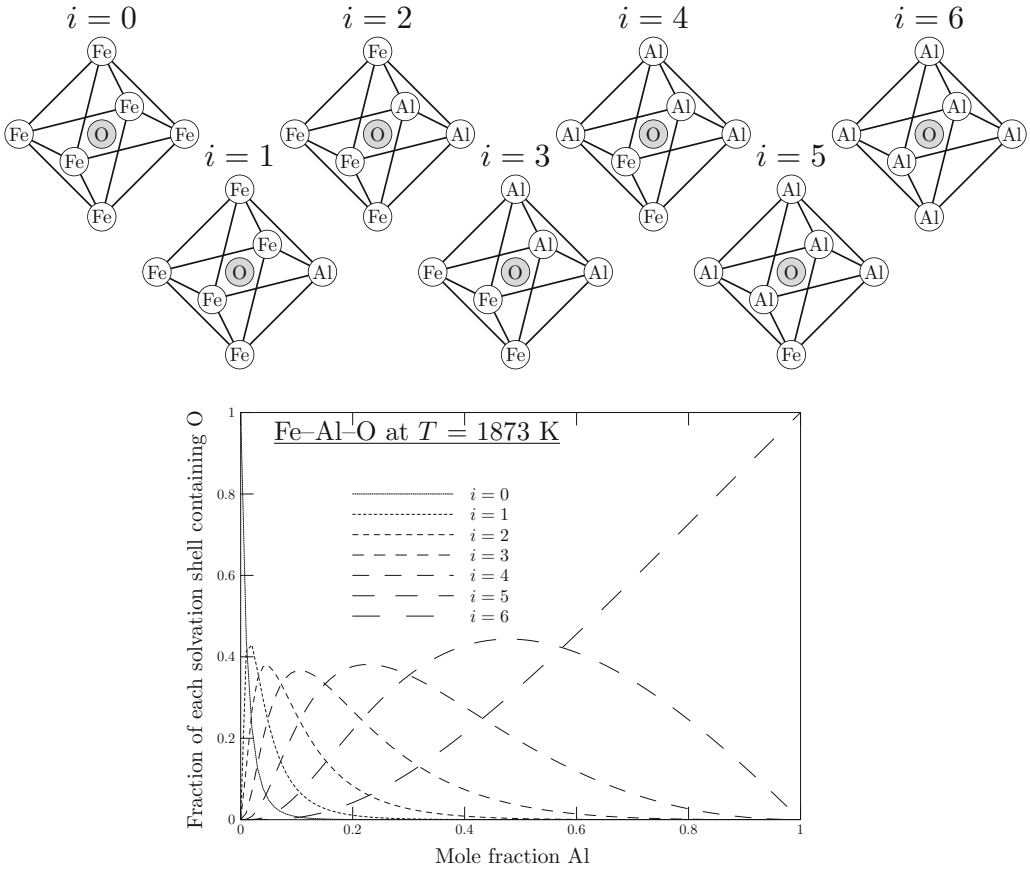

Fig. 6—Distribution of various solvation shells containing O as a function of Al content in the Fe-Al-O alloy at 1873 K (1600 °C) calculated in the present study (Eqs. [27] and [35]) at $X_O = 10^{-5.35}$.

Table III. Gibbs Energy of Dissolution of O in Liquid *M* at 1 At Pct ($\Delta g^{\circ}_{\underline{O}(M)}$) at 1873 K (1600 °C)

	References									
M	31	58	27	57	59	30	62	66	61	Estimation
Al	−414,246	−419,925		**−342,510**		−288,007				−395,292
B										−309,012
Ca	−464,844							−513,311		−398,927
Cr		**−200,970**			−205,927					−231,491
Fe	**−142,571**	−142,582	−142,659	−70,888						N.A.
Mg								−491,459		−358540
Mn	−222,518	−249,245			−212,015				−222518	**−210,853**
Nb	−273,900	−273,850			−227,104					**−288,309**
Si	−317,800	−317,765				−221,399	**−217,704***			−350,340
Ta					−229,617					**−332,284**
Ti	−389,608	−384,730			−369,210					**−373,920**
V	−302,613	−319,945			−247,652					−273,983
Zr	**−545156**				−413,772					−466,404

*Converted from 1 wt pct standard state by $\Delta g_{O(1\,wt\,pct \rightarrow 1\,at\,pct)} = RT\ln\frac{M_O}{M_{Si}}$ where M_O and M_{Si} are the atomic weight of O and Si, respectively

D. *Fe-Ca-O*

Comparison between the calculations and the experimental data in the Fe-Ca-O system is shown in Figure 8(b). The equilibrium oxide phase is CaO(s). Experimental data were taken from Kimura and Suito.[47] All the calculations predicted higher Ca content and lower O content than the experimental data.[47] Calculated solubility minima using the $\Delta g^{\circ}_{\underline{O}(Ca)}$ of Chang *et al.*[31] and the present estimation (Section IV–N) locate outside of the composition limit of the liquid alloy because of evaporation of Ca. Unfortunately, the present calculation does not explain the experimental data. This discrepancy will be discussed more in Section V–B.

Table IV. Equilibrium Constant of a Reaction $M_xO_y = xM(l) + \frac{y}{2}O_2(g)$ at 1873 K (1600 °C)

Reaction	$K_{M_xO_y}$ [45]
$Al_2O_3(s) = 2Al(l) + \frac{3}{2}O_2(g)$	1.0796×10^{-30}
$B_2O_3(l) = 2B(l) + \frac{3}{2}O_2(g)$	1.4089×10^{-24}
$CaO(s) = Ca(l) + \frac{1}{2}O_2(g)$	8.1330×10^{-13}
$Cr_2O_3(s) = 2Cr(l) + \frac{3}{2}O_2(g)$	4.4016×10^{-19}
$MgO(s) = Mg(l) + \frac{1}{2}O_2(g)$	1.1358×10^{-11}
$MnO(s) = Mn(l) + \frac{1}{2}O_2(g)$	1.7482×10^{-07}
$NbO_2(s) = Nb(l) + O_2(g)$	3.7135×10^{-14}
$SiO_2(s) = Si(l) + O_2(g)$	8.5451×10^{-17}
$Ta_2O_5(s) = 2Ta(l) + \frac{5}{2}O_2(g)$	1.9911×10^{-36}
$Ti_2O_3(s) = 2Ti(l) + \frac{3}{2}O_2(g)$	3.5332×10^{-29}
$V_2O_3(s) = 2V(l) + \frac{3}{2}O_2(g)$	4.2827×10^{-22}
$ZrO_2(s) = Zr(l) + O_2(g)$	9.9006×10^{-22}

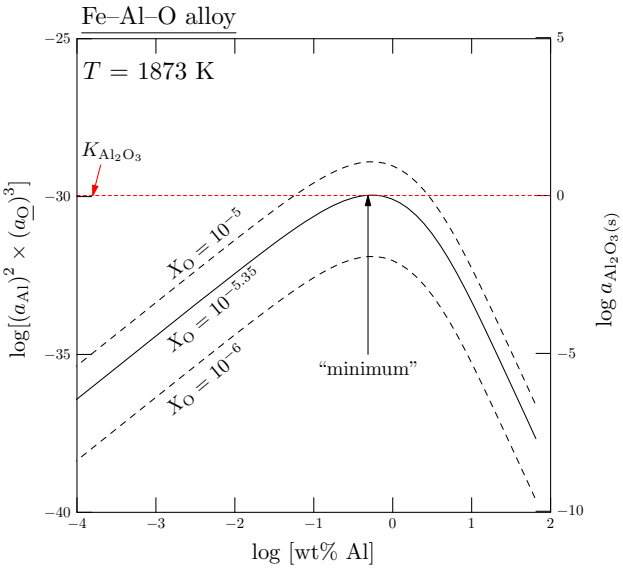

Fig. 7—Activity product of Fe-Al-O alloy at 1873 K (1600 °C) calculated in the present study (Eqs. [27] and [35]) at $X_O = 10^{-6}$, $10^{-5.35}$, and 10^{-5}.

E. *Fe-Cr-O*

Comparison between the calculations and the experimental data in the Fe-Cr-O system is shown in Figure 8(c). The equilibrium oxide phase is $Cr_2O_3(s)$. Experimental data were taken from Dimitrov *et al.*[48] The present calculations with various $\Delta g^\circ_{\underline{O}(Cr)}$ [58,59] including the estimated one in the present study are in favorable agreement with the experimental data.[48]

F. *Fe-Mg-O*

Comparison between the calculations and the experimental data in the Fe-Mg-O system is shown in Figure 8(d). The equilibrium oxide phase is MgO(s). Experimental data were taken from Seo and Kim.[49] All the calculations predicted higher Mg content and lower O content than the experimental data.[49] The calculated solubility minimum using the $\Delta g^\circ_{\underline{O}(Mg)}$ of the present estimation (Section IV–N) locates outside of the composition limit of the liquid alloy because of evaporation of Mg. As was the case for Fe-Ca-O, the present calculation does not explain the experimental data. This discrepancy will be discussed more in Section V–B.

G. *Fe-Mn-O*

Comparison between the calculations and the experimental data in the Fe-Mn-O system is shown in Figure 8(e). Equilibrium oxide phase is MnO(s)†. Experimental data were taken from Takahashi and Hino.[50] The present calculations with various $\Delta g^\circ_{\underline{O}(Mn)}$ [31,59,61] including the estimated one in the present study are in favorable agreement with the experimental data.[50]

†MnO forms a solid solution (Mn,Fe)O; therefore, the activity of the MnO(s) is not strictly at unity at equilibrium with a liquid Fe-Mn-O alloy. Therefore, the thermodynamic condition shown in Eq. [21] may need to be applied as:

$$\max(a_{Mn}a_{\underline{O}}) = K_{MnO} \times a_{MnO}$$

However, a_{MnO} is not significantly lower than unity (> 0.99[60]), and finding the Mn content at the solubility minimum is not sensitive to the right-hand side of the above equation.

H. *Fe-Nb-O*

Comparison between the calculations and the experimental data in the Fe-Nb-O system is shown in Figure 8(f). The equilibrium oxide phase is $NbO_2(s)$. Experimental data were taken from Gu and Tang.[51] The present calculations with various $\Delta g^\circ_{\underline{O}(Nb)}$ [31,58] including the estimated one in the present study are in favorable agreement with the experimental data.[51]

I. *Fe-Si-O*

Comparison between the calculations and the experimental data in the Fe-Si-O system is shown in Figure 8(g). Equilibrium oxide phase is $SiO_2(s)$. Experimental data were taken from Shibaev *et al.*[13] The present calculations with various $\Delta g^\circ_{\underline{O}(Si)}$ [30,62] are in favorable agreement with the experimental data.[13] Si content of the calculated minima locates at the upper limit of the experimental uncertainty of Shibaev *et al.*,[13] while the O content of the calculated minima is a few ppm higher than that of Shibaev *et al.*[13]

J. *Fe-Ta-O*

Comparison between the calculations and the experimental data in the Fe-Ta-O system is shown in Figure 8(h). Equilibrium oxide phase is $Ta_2O_{5(s)}$. Experimental data were taken from Fischer and Janke.[52] The calculation with the estimated $\Delta g^\circ_{\underline{O}(Ta)}$ in the present study is in favorable agreement with the experimental

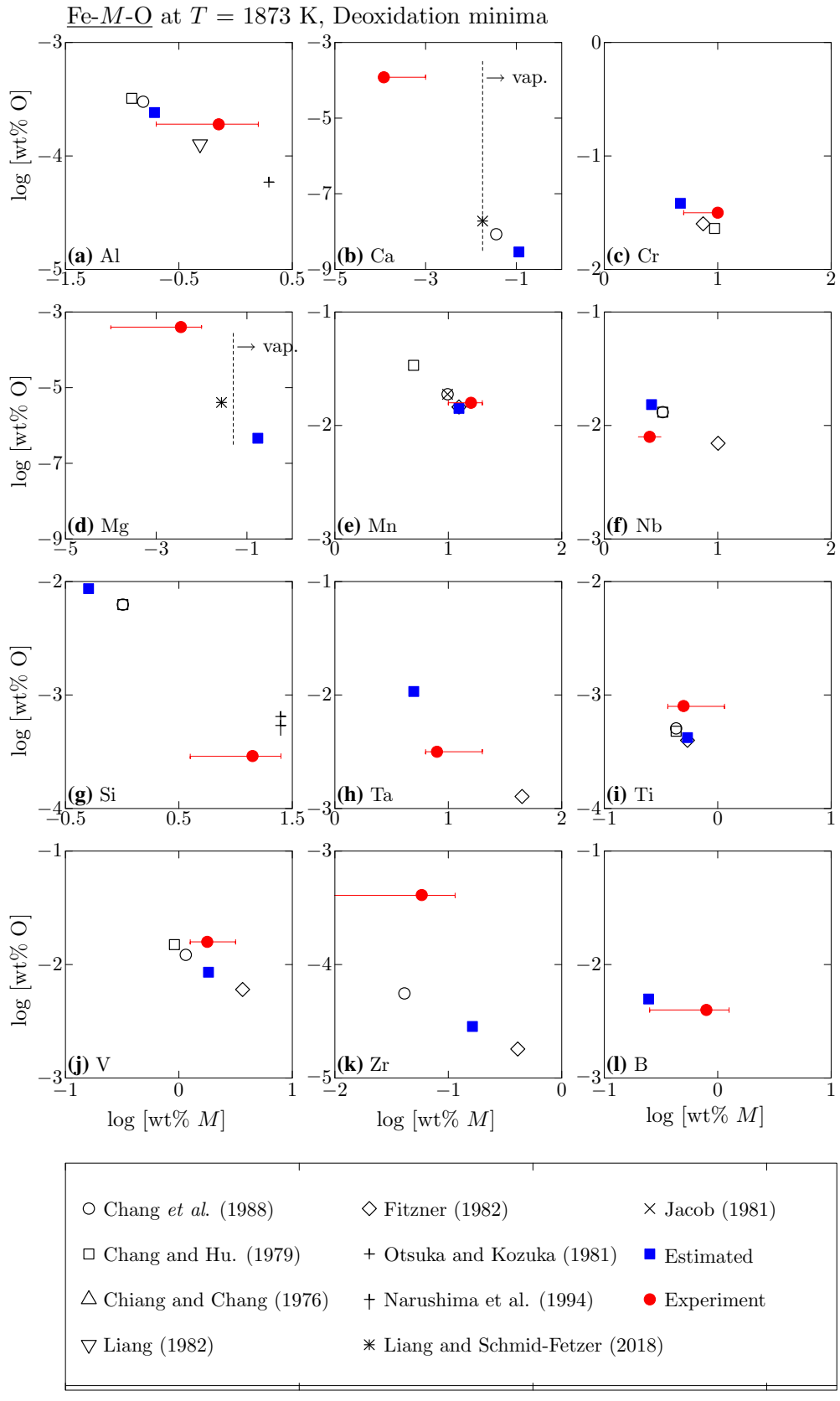

Fig. 8—Solubility minima of various Fe-*M*-O alloys at 1873 K (1600 °C): (*a*) Al, (*b*), Ca, (*c*), Cr, (*d*) Mg, (*e*) Mn, (*f*) Nb, (*g*) Si, (*h*) Ta, (*i*) Ti, (*j*) V, (*k*) Zr, and (*l*) B. Closed circles with error bar are the experimentally reported solubility minima. Other symbols are calculated in the present study (Eqs. [21], [27], [35] using various $\Delta g^{\circ}_{O_{(M)}}$). Dashed lines in (b) and (d) represent the upper limit of Ca and Mg contents due to vaporization at 1873 K (1600 °C), respectively.

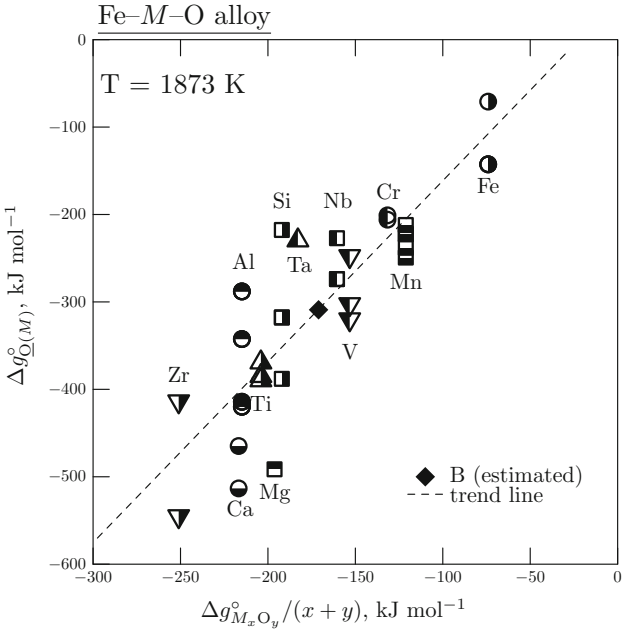

Fig. 9—Correlation between $\Delta g^\circ_{\underline{O}(M)}$ and $\Delta g^\circ_{M_xO_y}/(x+y)$ at 1873 K (1600 °C). Each symbol represents the data for each M. $\Delta g^\circ_{\underline{O}(B)}$ was estimated from the *trend line*.

data on Ta content, but gives a higher O content. The other calculation with $\Delta g^\circ_{\underline{O}(Ta)}$ available in the literature[59] predicts higher Ta and lower O contents, respectively.

K. *Fe-Ti-O*

Comparison between the calculations and the experimental data in the Fe-Ti-O system is shown in Figure 8(i). Equilibrium oxide phase is Ti_2O_3(s). Experimental data were taken from Cha *et al.*[53] The present calculations with various $\Delta g^\circ_{\underline{O}(Ti)}$[31,58,59] including the estimated one in the present study are in favorable agreement with the experimental data.[53]

L. *Fe-V-O*

Comparison between the calculations and the experimental data in the Fe-V-O system is shown in Figure 8(j). Equilibrium oxide phase is V_2O_3(s). Experimental data were taken from Kay *et al.*[54] The present calculations with various $\Delta g^\circ_{\underline{O}(V)}$,[31,58] including the estimated one in the present study, are in favorable agreement with the experimental data.[54]

M. *Fe-Zr-O*

Comparison between the calculations and the experimental data in the Fe-Zr-O system is shown in Figure 8(k). Equilibrium oxide phase is ZrO_2(s). Experimental data were taken from Inoue *et al.*[55] The present calculation with the $\Delta g^\circ_{\underline{O}(Zr)}$ available in the literature[31] is in favorable agreement with the experimental data on Zr content, but gives a lower O content.[55] Several cases have reported a discrepancy between significantly thermodynamic calculation and experimental data on the O content.[16,63] Experimentally determined O content is always higher than that predicted from thermodynamic calculations. This requires further investigation.

N. *Estimation of the Gibbs Energy of Dissolution of O in Liquid M ($\Delta g^\circ_{\underline{O}(M)}$)*

From the previous comparisons, it can be seen that the prediction of solubility minima depends on the $\Delta g^\circ_{\underline{O}(M)}$. It can also be inferred from Figure 3 that occurrence of a maximum in the activity product depends on the $\Delta g^\circ_{\underline{O}(M)}$ *via* interaction between M and O. Therefore, one should be careful when choosing the $\Delta g^\circ_{\underline{O}(M)}$ value. According to Jacob and others,[61,64,65] $\Delta g^\circ_{\underline{O}(M)}$ is known to be proportional to the standard enthalpy of formation of M_xO_y per mole of atoms. In the present study, all the $\Delta g^\circ_{\underline{O}(M)}$ found in the literature were plotted as a function of the standard Gibbs energy of formation of M_xO_y ($\Delta g^\circ_{M_xO_y} = -RT\ln K_{M_xO_y}$) per mole of atoms, as shown in Figure 9. Each symbol represents $\Delta g^\circ_{\underline{O}(M)}$ available in the literature for each metallic element M. There is a noticeable correlation between the two terms, although scatters in the $\Delta g^\circ_{\underline{O}(M)}$ values available are not negligible. Nevertheless, the best correlation was attempted by regression and is shown by the dashed line: $\Delta g^\circ_{\underline{O}(M)}$ (J mol^{-1}) = $1.9673 \times \frac{\Delta g^\circ_{M_xO_y}}{(x+y)}$ + 27,484 (J mol^{-1}). For each M, $\Delta g^\circ_{\underline{O}(M)}$ was also estimated by the "trend line;" the solubility minima were calculated and are shown in Figure 8 by the solid squares. This correlation may be used when $\Delta g^\circ_{\underline{O}(M)}$ at 1873 K (1600 °C) is not available in the literature.

O. *Fe-B-O*

To the best knowledge of the present author, no data were reported for $\Delta g^\circ_{\underline{O}(B)}$. From Figure 9, it could be estimated to be $-309,011$ J mol^{-1} at 1873 K (1600 °C). This value was used to predict the solubility minimum of B_2O_3 (this is liquid at 1873 K (1600 °C)), as shown in Figure 8(l) with available experimental data.[52] The present calculations with the estimated $\Delta g^\circ_{\underline{O}(B)}$ are in favorable agreement with the experimental data.[52] However, due to a considerable scatter in Figure 9, this correlation may only be used for a qualitative estimation purpose.

V. DISCUSSION

All the best-predicted solubility minima at 1873 K (1600 °C) are shown in Figure 10 with the references of $\Delta g^\circ_{\underline{O}(M)}$ used in each calculation. Those used in the calculation out of all the available $\Delta g^\circ_{\underline{O}(M)}$ values are marked in **bold** in Table III, except for those of Ca and Mg.

A. *Properties Determining the Solubility Minima*

Half of the minima shown in Figure 10 (M = Mn, Cr, Ta, Nb, V, and B) show that their minimum O contents at 1873 K (1600 °C) are roughly located near 0.01 wt pct, while those of Si, Ti, and Al are in the range of 0.001 to 0.0001 wt pct. Those of Zr, Mg, and Ca are even < 0.0001 wt pct, which is thought to be lower than the detection limit of the conventional O analysis method (inert gas/vacuum fusion infrared absorption method). On the other hand, M contents at the minima are widely spread.

Interestingly, Al and Ti have similar $\Delta g^\circ_{\underline{O}(M)}$ and $\Delta g^\circ_{M_xO_y}/(x+y)$, and their solubility minima are close to each other. Cr and Mn, Nb, and V also have similar $\Delta g^\circ_{\underline{O}(M)}$ and $\Delta g^\circ_{M_xO_y}/(x+y)$, and their solubility minima are close to each other, respectively. It is inferred from these observations that $\Delta g^\circ_{\underline{O}(M)}$ and $\Delta g^\circ_{M_xO_y}/(x+y)$ are likely the determining factors of the solubility minima, apart from the interaction between Fe and M, which is weaker than the interaction between M (and Fe) and O.

As shown in Figure 9 as well as the previous reports by Jacob and others,[61,64,65] the Gibbs energy of formation (or enthalpy of formation) of M_xO_y ($\Delta g^\circ_{M_xO_y}$) is roughly proportional to the Gibbs energy of dissolution of O in liquid metal M ($\Delta g^\circ_{\underline{O}(M)}$). However, in the present study, it was found that $\Delta g^\circ_{\underline{O}(M)}$ is more correlated to the M content at the minima ([wt pctM]$_{min}$), while $\Delta g^\circ_{M_xO_y}$ is more correlated to the O content at the minima ([wt pct O]$_{min}$). This is shown in Figure 11. All the data were those from Figures 9 and 10.

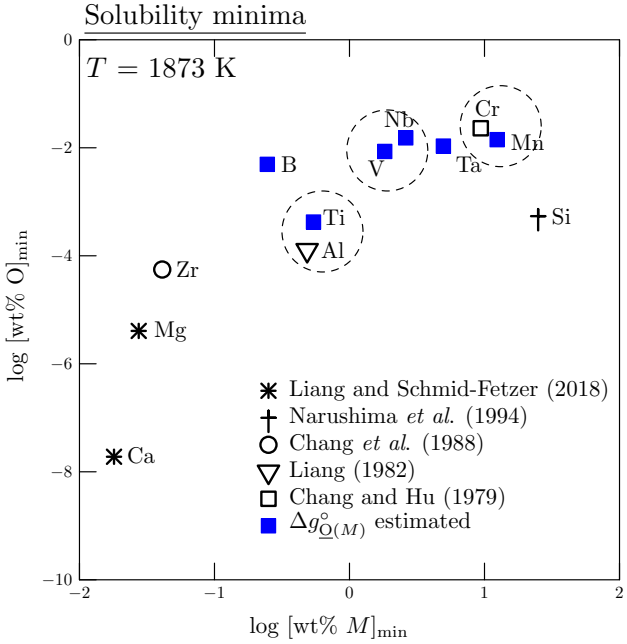

Fig. 10—Predicted minimum solubilities of M_xO_y in liquid Fe-M-O alloys at 1873 K (1600 °C). $\Delta g^\circ_{\underline{O}(M)}$ used in those predictions were taken from Refs. 31, 57, 58, 62, 66 or estimation in the present study.

Since the solubility minimum is determined by the maximum of the activity product, the composition dependence of $\gamma_{\underline{O}}$ is important in determining the solubility minimum. Shown in Figure 12 is the calculated $\log \gamma_{\underline{O}}$ in the Fe-M alloys at 1873 K (1600 °C) using Eq. [35] and $\Delta g^\circ_{\underline{O}(M)}$ marked bold in Table III. "m" in each figure indicates the [wt pct M]$_{min}$ in each case. Upon increasing [wt pct M], the $\gamma_{\underline{O}}$ first keeps its value close to $\gamma_{\underline{O}(Fe)}$, then decreases toward $\gamma_{\underline{O}(M)}$. It can be seen approximately that the $\gamma_{\underline{O}}$ starts to decrease near the "m." Moreover, those "m"s shift to higher [wt pct M] if $\Delta g^\circ_{\underline{O}(M)}$ is less negative.

An interesting case is the solubility of SiO_2 in liquid Fe-Si-O alloy. The solubility minimum of SiO_2 is located at the highest [wt pct M]$_{min}$ among the other elements, but [wt pct O]$_{min}$ is not as high as that of MnO or Cr_2O_3 whose [wt pct M]$_{min}$ are also high (see Figure 10). Figure 11 shows that $\Delta g^\circ_{\underline{O}(Si)}$ is almost comparable to those of Cr and Mn, but $\Delta g^\circ_{SiO_2}/3$ is significantly more negative than $\Delta g^\circ_{MnO}/2$ or $\Delta g^\circ_{Cr_2O_3}/5$. This results in similar [wt pct M]$_{min}$ but lower [wt pct O]$_{min}$ in case of SiO_2 solubility.

It is now understood that, upon increasing the M content, a rapid decrease of the $\gamma_{\underline{O}}$ due to negative $\Delta g^\circ_{\underline{O}(M)}$ results in shifting the maximum of the activity product toward lower M content (and *vice versa*). The lower $K_{M_xO_y}$ yields lower $a_{\underline{O}}$ and X_O at the critical activity product (and *vice versa*). The role of the interaction between the metallic components (g^{ex}) seems not as significant as those of $\Delta g^\circ_{\underline{O}(M)}$ and $K_{M_xO_y}$, in particular for the calculation of $\gamma_{\underline{O}}$. This seems generally valid as the extent of interaction between the metallic components is weaker than that between the metal (Fe and M) and O. However, this does not mean that the g^{ex} can be neglected in the present calculation, because the a_M should be calculated as accurately as possible.

B. *Solubility Minima of CaO and MgO*

The solubility minima of CaO and MgO were not predicted satisfactorily (Figures 8(b) and (d), respectively). The predicted minima were located at higher Ca/Mg content and lower O content. Because the experiments for the solubility measurement of CaO and MgO in liquid Fe are extremely difficult (because of high temperature, evaporation of the Ca and Mg, the extremely strong affinity of Ca and Mg to O that lowers the O content below detection limit), careful evaluation of the experimental data is required. Nevertheless, if the selected experimental data (closed circles in Figure 8) are accepted, then the present calculation seems to show a limit in the prediction of the solubility minima.

According to Figure 12(c) and the conclusion derived in Section V–A, it is seen that $\gamma_{\underline{O}}$ decreases as the Ca content increases, but not as quickly as it is supposed to. That is, $\gamma_{\underline{O}}$ needs to start to decrease at a lower Ca content in order to have a maximum of the activity product at the lower Ca content and needs to have a

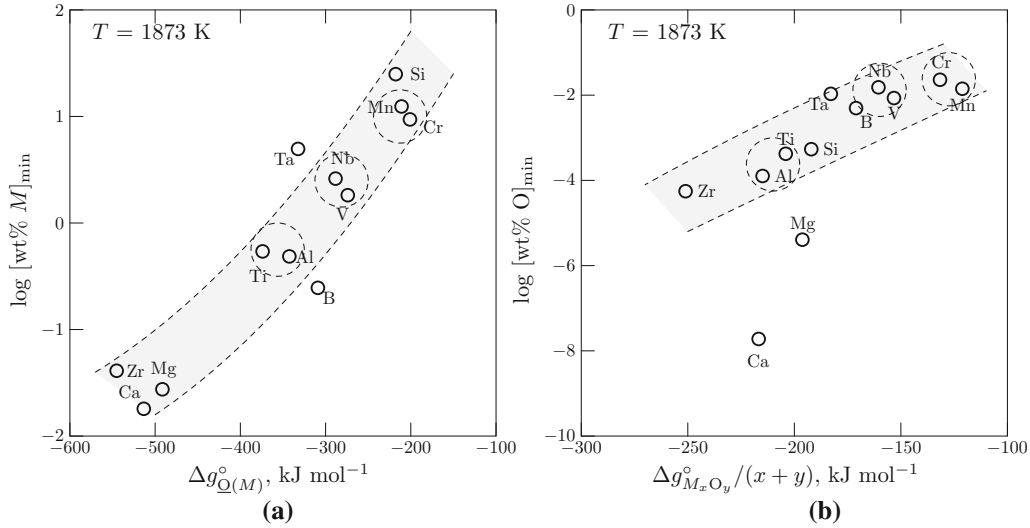

Fig. 11—Properties impacting on the solubility minima: (a) dependence of $[\text{wt pct}M]_{\text{min}}$ on $g^{\circ}_{\underline{O}(M)}$; (b) dependence of $[\text{wt pctO}]_{\text{min}}$ on $\Delta g^{\circ}_{M_xO_y}/(x+y)$.

lower $\gamma_{\underline{O}}$ that yields a higher O content at the solubility minimum. To decrease the $\gamma_{\underline{O}}$ more quickly upon increasing the Ca content, it is necessary to analyze Eq. [35] to determine whether it is suitable to describe the solvation shell of O composed of Fe-Ca. Since the solvation reaction (Eq. [32] or Eq. [33]) represents the transfer of O in the solvation shells from lower to higher Ca content, $\Delta h_{(i)}$ in this case is negative. According to Wagner's interpretation of $h(=\Delta h_{(i+1)}-\Delta h_{(i)})$,[26] increasing Ca content (by increasing i) in the solvation shell gradually decreases the extent of O dissolution in the solvation shell (the transfer of electrons from Ca to O over the transfer of electrons from Fe to O). That is, Reaction [33] is less exothermic than Reaction [32], thereby $h>0$. In Wagner's original model, the h was assumed to be a constant in each binary liquid. This was later modified by Chiang and Chang in such a way that $h=h_1+h_2\times i$.[27] In the present study, this expression was not adopted because it requires parameter assessment, which was out of the scope of the present study. Schmid *et al.* proposed considering the non-random mixing of the metallic atoms in the solvation shell model: Eq. [34] instead of Eq. [35] by setting $h_{\text{Fe}M}\neq 0$. A preliminary test of the non-random solvation shell model (Eq. [34])[28] yielded a better result than the random solvation shell model (Eq. [35])[26] for the case of CaO solubility. A similar improvement was observed in the case of MgO solubility. However, the same approach did not yield such improvement in cases of Al_2O_3 solubility and ZrO_2 solubility, where Al and Zr also showed a strong affinity to the O, comparable to those of Ca and Mg. Interestingly, binary liquid alloys of Fe-Ca and Fe-Mg exhibited very strong positive deviation from the ideality (forming immiscibility), while those of Fe-Al and Fe-Zr exhibited negative deviation (see Table I). This may be responsible for the different behaviors when the non-random solvation shell model was applied. Further investigation is required.

VI. CONCLUSION

Minima of oxide solubility in various liquid Fe-M-O alloys were analyzed. The origin of the solubility minimum was interpreted not by tracking a minimum of the solubility curve as was done previously, but by looking at the driving force to form the oxide (M_xO_y) in terms of activity product ($a_M^x\times a_{\underline{O}}^y$). It was shown that, at a given O content in a liquid Fe-M-O alloy, a_M increases and $a_{\underline{O}}$ decreases upon increasing the M content. This results in a maximum in the activity product. When the activity product at its maximum equals $K_{M_xO_y}$, the composition (M and O contents) corresponds to the solubility minimum of the pure M_xO_y. At higher M content than that of the solubility minimum, the activity product decreases because of the decrease of $a_{\underline{O}}$. This results from the strong affinity of M to O, which causes more O to dissolve in the liquid alloy. Therefore, the solubility limit of the M_xO_y increases back after the solubility minimum.

The idea of the solubility minimum was applied to *predict* the actual solubility minima of M_xO_y in various Fe-M-O alloys at 1873 K (1600 °C) where M = Al, B, Ca, Cr, Mg, Mn, Nb, Si, Ta, Ti, V, and Zr. A number of assessed CALPHAD Gibbs energy equations were used to obtain a_M over the whole composition (from pure Fe to pure M). Wagner's solvation shell model[26] with Chiang and Chang's parameterization for h[58] was used to obtain $a_{\underline{O}}$ over the whole composition but in the dilute region of O. The predicted (not *fitted*) solubility minima were in favorable agreement with reported experimental data, except for those of CaO and MgO. There were correlations between $[\text{wt pct M}]_{\text{min}}$ and $\Delta g^{\circ}_{\underline{O}(M)}$, also between $[\text{wt pct O}]_{\text{min}}$ and $\Delta g^{\circ}_{M_xO_y}/(x+y)$, respectively. Therefore, similar $\Delta g^{\circ}_{\underline{O}(M)}$ and $\Delta g^{\circ}_{M_xO_y}/(x+y)$ result in a similar composition of solubility minima. For systems where $\Delta g^{\circ}_{\underline{O}(M)}$ is

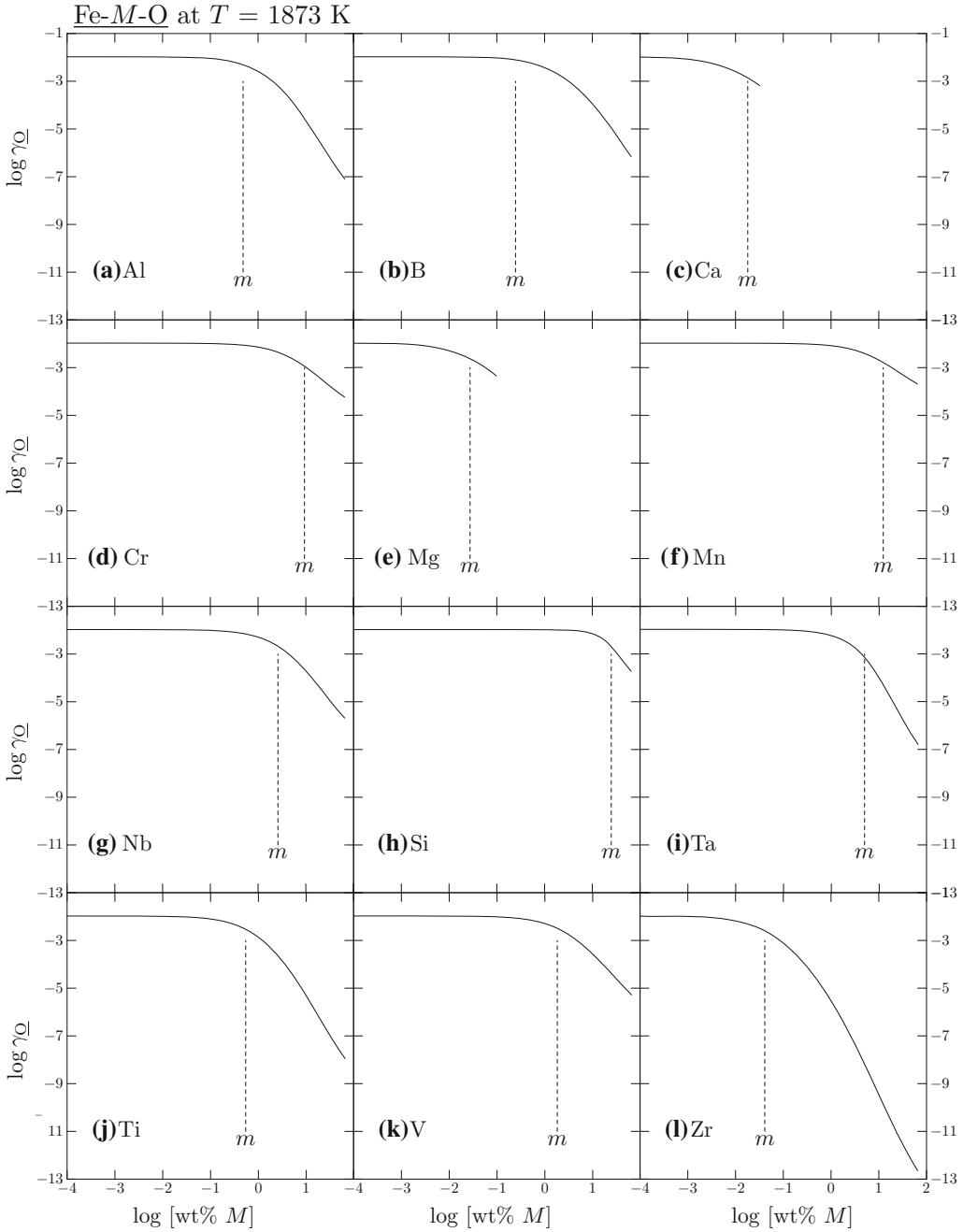

Fig. 12—$\log \gamma_{\underline{O}}$ in liquid Fe-*M*-O alloys as a function of [wt pct *M*]: (*a*) Al, (*b*) B, (*c*) Ca, (*d*) Cr, (*e*) Mg, (*f*) Mn, (*g*) Nb, (*h*) Si (*i*) Ta, (*j*) Ti, (*k*) V, and (*l*) Zr. It is virtually the Henrian activity coefficient of O in the liquid Fe-*M* alloy (γ°_{O}). The $\log \gamma_{\underline{O}}$ in Fe-Ca-O and in Fe-Mg-O alloys were plotted up to the upper limit of immiscibility.

not known, a correlation obtained between $\Delta g^{\circ}_{\underline{O}(M)}$ and $\Delta g^{\circ}_{M_xO_y}/(x+y)$ may be used. However, due to a considerable scatter, this correlation can only be used for qualitative estimation purposes.

ACKNOWLEDGEMENTS

The present author is grateful for the hospitality of Prof. P. Chartrand, École Polytechnique de Montréal, Canada, during his sabbatical stay. Constructive comments from Prof. Emeritus A.D. Pelton, École Polytechnique de Montréal, Canada, are also appreciated.

REFERENCES

1. C. Wagner: *Thermodynamics of Alloys*, Addison-Wesley Pub. Co., Reading, MA, 1951, pp. 51–53.
2. G. Sigworth and J.F. Elliott: *Met. Sci.*, 1974, vol. 8, pp. 298–310.
3. Japan Society for the Promotion of Science: in *Steelmaking Data Sourcebook*, Gordon & Breach Science, New York, NY, 1988.

4. C. Lupis: in *Chemical Thermodynamics of Materials*, Simon & Schuster (Asia) Pte Ltd, Singapore, 1993.
5. J. D'Entremont, D. Guernsey, and J. Chipman: *Trans. Metall. Soc. AIME*, 1963, vol. 227, pp. 14–17.
6. V. Shevtsov: *Russ. Metall.*, 1981, vol. 1, pp. 52–57.
7. G.R.S. Pierre and R. Blackburn: *Trans. Metall. Soc. AIME*, 1968, vol. 242, pp. 2–4.
8. G.R.S. Pierre: *Metall. Trans. B*, 1977, vol. 8, pp. 215–17.
9. P.-W. Han, P.-X. Chen, and S.-J. Chu: *High Temp. Mater. Proc.*, 2016, vol. 35, pp. 347–51.
10. M. Hone, S. Houot, and M. Rigaud: *Can. Metall. Quart.*, 1974, vol. 13, pp. 619–23.
11. C.-G. Kuo: *J. Alloys Compd.*, 2010, vol. 494, pp. 72–77.
12. G.R. Holcomb and G.R.S. Pierre: *Metall. Trans. B*, 1992, vol. 23, pp. 789–90.
13. S.S. Shibaev, P.V. Krasovskii, and K.V. Grigorovitch: *ISIJ Int.*, 2005, vol. 45, pp. 1243–47.
14. H. Itoh, M. Hino, and S. Ban-Ya: *Tetsu-to-Hagane*, 1997, vol. 83, pp. 773–78.
15. D. Bouchard and C.W. Bale: *J. Phase Equilib.*, 1995, vol. 16, pp. 16–23.
16. I.-H. Jung, S. Decterov, and A.D. Pelton: *Metall. Mater. Trans. B*, 2004, vol. 35B, pp. 493–507.
17. C.W. Bale and A.D. Pelton: *Metall. Mater. Trans. A*, 1990, vol. 21A, pp. 1997–2002.
18. A.D. Pelton: *Metall. Mater. Trans. B*, 1997, vol. 28, pp. 869–76.
19. M.-K. Paek, J.-J. Pak, and Y.-B. Kang: *Metall. Mater. Trans. B*, 2015, vol. 46, pp. 2224–33.
20. A.D. Pelton, S.A. Degterov, G. Eriksson, C. Robelin, and Y. Dessureault: *Metall. Mater. Trans. B*, 2000, vol. 31B, pp. 651–59.
21. M.-K. Paek, J.-M. Jang, Y.-B. Kang, and J.-J. Pak: *Metall. Mater. Trans. B*, 2015, vol. 46B, pp. 1826–36.
22. A.D. Pelton and P. Chartrand: *Metall. Mater. Trans. A*, 2001, vol. 32, pp. 1355–60.
23. G. Eriksson and A.D. Pelton: *Metall. Trans. B*, 1993, vol. 24, pp. 807–16.
24. D. Janke and W. Fischer: *Arch. Eisenhüttenwes*, 1976, vol. 47, pp. 195–98.
25. M.-K. Paek, K.-H. Do, Y.-B. Kang, I.-H. Jung, and J.-J. Pak: *Metall. Mater. Trans. B*, 2016, vol. 47, pp. 2837–47.
26. C. Wagner: *Acta Metall.*, 1973, vol. 21, pp. 1297–1303.
27. T. Chiang and Y.A. Chang: *Metall. Trans. B*, 1976, vol. 7, pp. 453–67.
28. R. Schmid, J.-C. Lin, and Y.A. Chang: *Zeit. fuer Metall.*, 1984, vol. 75, pp. 730–37.
29. L. Pauling: *The Nature of the Chemical Bond*, Cornell University Press, Ithaca, NY, 1970.
30. S. Otsuka and Z. Kozuka: *Metall. Trans. B*, 1981, vol. 12, pp. 455–59.
31. Y.A. Chang, K. Fitzner, and M.-X. Zhang: *Prog. Mater. Sci.*, 1988, vol. 32, pp. 97–259.
32. R. Hultgren, P. Desai, D. Hawkins, M. Gleiser, and K. Kelley: *Selected Values of Thermodynamic Properties of Binary Alloys*, ASM, Metals Park, OH, 1973.
33. B. Sundman, I. Ohnuma, N. Dupin, U.R. Kattner, and S.G. Fries: *Acta Mater.*, 2009, vol. 57, pp. 2896–2908.
34. B. Hallemans, P. Wollants, and J.R. Roos: *J. Phase Equilib.*, 1995, vol. 16, pp. 137–49.
35. M. Selleby and B. Sundman: *Calphad*, 1996, vol. 20, pp. 381–92.
36. J.-O. Andersson and B. Sundman: *Calphad*, 1987, vol. 11, pp. 83–92.
37. J. Tibballs: in *System Fe-Mg*, European Communities, 1998, pp. 195–196.
38. W. Huang: *Calphad*, 1989, vol. 13, pp. 243–52.
39. S. Liu, B. Hallstedt, D. Music, and Y. Du: *Calphad*, 2012, vol. 38, pp. 43–58.
40. J. Lacaze and B. Sundman: *Metall. Trans. A*, 1991, vol. 22, pp. 2211–23.
41. S. Srikanth and A. Petric: *J. Alloys Compd.*, 1994, vol. 203, pp. 281–88.
42. J. De Keyzer, G. Cacciamani, N. Dupin, and P. Wollants: *Calphad*, 2009, vol. 33, pp. 109–23.
43. K. Hari Kumar and V. Raghavan: *Calphad*, 1991, vol. 15, pp. 307–14.
44. M. Jiang, K. Oikawa, T. Ikeshoji, L. Wulff, and K. Ishida: *J. Phase Equilib.*, 2001, vol. 22, pp. 406–17.
45. C.W. Bale, E. Bélisle, P. Chartrand, S.A. Decterov, G. Eriksson, A.E. Gheribi, K. Hack, I.H. Jung, Y.B. Kang, J. Melançon, A.D. Pelton, S. Petersen, C. Robelin, J. Sangster, P. Spencer, and M.-A. Van Ende: *Calphad*, 2016, vol. 54, pp. 35–53.
46. M. Chase, ed.: in *JANAF Thermochemical Tables*, AIP, Woodbury, NY, 1985.
47. T. Kimura and H. Suito: *Metall. Mater. Trans. B*, 1994, vol. 25B, pp. 33–42.
48. S. Dimitrov, H. Venz, K. Koch, and D. Janke: *Steel Res.*, 1995, vol. 66, pp. 39–43.
49. J.-D. Seo and S.-H. Kim: *Steel Res.*, 2000, vol. 71, pp. 101–106.
50. K. Takahashi and M. Hino: *High Temp. Mater. Proc.*, 2000, vol. 19, pp. 1–10.
51. L. Gu and Z. Tang: *Acta Metall. Sin.*, 1985, vol. 21, pp. A167–74.
52. W. Fischer and D. Janke: *Arch. Eisenhüttenwes*, 1971, vol. 42, pp. 695–98.
53. W.-Y. Cha, T. Nagasaka, T. Miki, Y. Sasaki, and M. Hino: *ISIJ Int.*, 2006, vol. 46, pp. 996–1005.
54. D. Kay and A. Kontopoulos, in *Chemical Metallurgy of Iron and Steel: Proc. Int. Symp on Metallurgical Chemistry—Application in Ferrous Metallurgy, Iron and Steel Institute*, London, 1971, pp. 178–183.
55. R. Inoue, T. Ariyama, and H. Suito: *ISIJ Int.*, 2008, vol. 48, pp. 1175–81.
56. A. Ghosh and G. Murthy: *Trans. ISIJ*, 1986, vol. 26, pp. 629–37.
57. W. Liang: *Zeit. fuer Metall.*, 1982, vol. 73, pp. 369–75.
58. Y.A. Chang and D.C. Hu: *Metall. Trans. B*, 1979, vol. 10, pp. 43–48.
59. K. Fitzner: *Thermochim. Acta*, 1982, vol. 52, pp. 103–11.
60. Y.-B. Kang and I.-H. Jung: *J. Phys. Chem. Solids*, 2016, vol. 98, pp. 237–46.
61. K.T. Jacob: *Metall. Trans. B*, 1981, vol. 12, pp. 675–78.
62. T. Narushima, K. Matsuzawa, Y. Mukai, and Y. Iguchi: *Mater. Trans. JIM*, 1994, vol. 35, pp. 522–28.
63. W. Huang: *Calphad*, 2004, vol. 28, pp. 153–57.
64. K. Jacob and C. Alcock: *Acta Metall.*, 1972, vol. 20, pp. 221–32.
65. K. Fitzner and K. Jacob: *J. Less Common Met.*, 1977, vol. 52, pp. 279–91.
66. S.-M. Liang and R. Schmid-Fetzer: *J. Eur. Ceram. Soc.*, 2018, vol. 38, pp. 4768–85.